ACS OMEGA

http://pubs.acs.org/journal/acsodf

Article

Effects of a Nanophase-Separated Structure on Mechanical Properties and Proton Conductivity of Acid-Infiltrated Block Polymer Electrolyte Membranes under Non-Humidification

Takato Kajita, Haruka Tanaka, Yumiko Ohtsuka, Tsuyoshi Orido, Atsushi Takano, Hiroyuki Iwamoto, Albert Mufundirwa, Hideto Imai, and Atsushi Noro*

Cite This: *ACS Omega* 2023, 8, 1121−1130

Read Online

ACCESS | Metrics & More | Article Recommendations | Supporting Information

ABSTRACT: Acid-infiltrated block polymer electrolyte membranes adopting a spherical or lamellar nanophase-separated structure were prepared by infiltrating sulfuric acid (H_2SO_4) into polystyrene-*b*-poly(4-vinylpyridine)-*b*-polystyrene (S−P−S) triblock copolymers to investigate the effects of its nanophase-separated structure on mechanical properties and proton conductivities under non-humidification. Lamellae-forming S−P−S/H_2SO_4 membranes with a continuous hard phase generally exhibited higher tensile strength than sphere-forming S−P−S/H_2SO_4 membranes with a discontinuous hard phase even if the same amount of Sa was infiltrated into each neat S−P−S film. Meanwhile, the conductivities of lamellae-forming S−P−S/H_2SO_4 membranes under non-humidification were comparable or superior to those of sphere-forming S−P−S/H_2SO_4 membranes, even though they were infiltrated by the same weight fraction of H_2SO_4. This result is attributed to the conductivities of S−P−S/H_2SO_4 membranes being greatly influenced by the acid/base stoichiometry associated with acid−base complex formation rather than the nanophase-separated structure adopted in the membranes. Namely, there are more free H_2SO_4 moieties that can release free protons contributing to the conductivity in lamellae-forming S−P−S/H_2SO_4 membranes than sphere-forming S−P−S/H_2SO_4, even when the same amount of H_2SO_4 was infiltrated into the S−P−S.

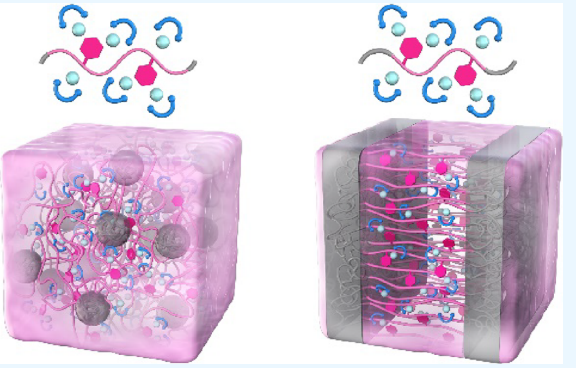

1. INTRODUCTION

Fuel cells generate electrical energy through an electrochemical reaction between hydrogen and oxygen gases, producing only water as a product; therefore, these cells are promising as clean power generation systems.[1,2] Polymer electrolyte fuel cells (PEFCs) using proton-conductive polymer electrolyte membranes (PEMs) consisting of the important components in fuel cells are operated at relatively low temperatures, approximately 70−90 °C,[3−12] as compared with other fuel cells based on other electrolytes such as solid oxides and phosphoric acid, which are typically operated at 200 °C or higher; thus, PEFCs can be used in a limited space such as fuel cell vehicles[6] and household fuel cell cogeneration systems.[7] The most well-known proton-conductive PEM is a perfluorosulfonic acid polymer such as Nafion.[8,9] Nafion exhibits high proton conductivities of 0.05 S cm^{-1} at 80 °C and 70 %RH, and 0.1 S cm^{-1} at 80 °C and 90 %RH,[10] where the fluorinated phase contributing to the mechanical strength of a membrane is separated from the proton-conductive sulfonic acid group/water mixed phase at a microscopic scale.[11,12] However, Nafion exhibits almost no conductivity under non-humidification; therefore, a PEFC using Nafion requires a system that controls not only temperature but also humidity.

To address the abovementioned problem, PEMs exhibiting proton conductivities even under non-humidification have been widely studied.[13−31] A representative example of proton-conductive PEMs that can be operated under non-humidification is a phosphoric acid-doped polybenzimidazole (PBI) membrane, where PBI is a type of super-engineered plastic with aromatic rings in the backbone. At an early stage in development of phosphoric acid-doped PBI membranes, the conductivity was ∼0.04 S cm^{-1} at a relatively high temperature of 190 °C under non-humidification for the membrane with 61 wt % phosphoric acid of a low-molecular-weight electrolyte.[13] Further development allowed the preparation of PBI with 93 wt % phosphoric acid exhibiting a high conductivity (0.16 S cm^{-1}) at 120 °C under dry conditions via a sol−gel process by heating the monomer of PBI with polyphosphoric acid.[16] As

Received: October 10, 2022
Accepted: December 12, 2022
Published: December 22, 2022

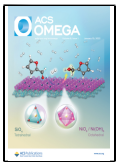

https://doi.org/10.1021/acsomega.2c06514
ACS Omega 2023, 8, 1121−1130

other PEMs, an ionic liquid (IL)-doped PBI membrane[17,19] and an IL-doped sulfonated polyimide membrane[20] have also been reported; however, they exhibited lower conductivities than the phosphoric acid-doped PBI membranes because the conductivities of neat phosphoric acid[32] under non-humidification are typically higher than those of neat ILs.[33]

Vinyl polymer-based PEMs have also been developed as further alternatives of proton-conductive PEMs under non-humidification.[34−43] For example, Narayanan and coworkers prepared a PEM by infiltrating sulfuric acid (H_2SO_4) or phosphoric acid into poly(4-vinylpyridine) with a basic group,[35] although the conductivity of the PEM with 48 wt % H_2SO_4 was a mere $\sim 2 \times 10^{-4}$ S cm^{-1} at 140 °C under non-humidification. To attain higher conductivities, the amount of infiltrated H_2SO_4 contributing to high proton conduction[44] should be larger, but the mixture of poly(4-vinylpyridine) and a larger amount of H_2SO_4 easily becomes a fluid because the glass transition temperature (T_g) of such a mixture tends to be lower than the operation temperature. Therefore, to keep the mixture of poly(4-vinylpyridine) and H_2SO_4 solid, we have recently prepared a proton-conductive PEM by chemically cross-linking poly(4-vinylpyridine), which can be swollen with a large amount of H_2SO_4, exhibiting conductivities over 0.1 S cm^{-1} at around 100 °C under non-humidification.[42] A highly proton-conductive PEM under non-humidification has also been prepared by infiltrating H_2SO_4 into a nanophase-separated polystyrene-*b*-poly(4-vinylpyridine)-*b*-polystyrene (S−P−S) triblock copolymer that can be prepared by living addition polymerization[45,46] of vinyl monomers. The effect of the acidity of the specific acid (H_2SO_4 or phosphoric acid) on the conductivity of the S−P−S/acid membranes was evaluated as well, revealing that H_2SO_4 was more effective in preparing highly conductive acid-infiltrated PEMs than phosphoric acid.[43]

Depending on the composition of block polymers, nanophase-separated structures of block polymers vary from a spherical structure with isolated discontinuous spheres in a continuous matrix to a lamellar structure with stacked continuous layers.[47,48] If nanophase-separated structures formed in PEMs of acid-infiltrated block polymers are different, the PEMs should also exhibit different conductivities and mechanical properties. To date, the effects of the nanophase-separated structure, probably one of the key factors determining the properties of PEMs of acid-infiltrated block polymers, has not been sufficiently investigated. Therefore, in this study, block polymer-based PEMs infiltrated with H_2SO_4 have been prepared by using two S−P−S triblock copolymers adopting different nanophase-separated structures with different phase continuities (Figure 1) to investigate the effects of a phase-separated structure on the mechanical properties and conductivities of the PEMs under non-humidification. The effects of H_2SO_4 weight fraction in the PEMs are also investigated. The study uses H_2SO_4 as an infiltrated acid since block polymer-based PEMs infiltrated with H_2SO_4 are expected to exhibit higher conductivities under non-humidification than block polymer-based PEMs infiltrated with phosphoric acid when the amount of infiltrated acid is the same.[43] It should also be noted that S−P−S triblock copolymers were used instead of S-P diblock copolymers because S−P−S triblock copolymer-based membranes exhibit better mechanical properties than S−P diblock copolymer-based membranes due to formation of polymer network by bridging P center blocks with the hard S domains in the S−P−S triblock copolymer-based membranes.[49]

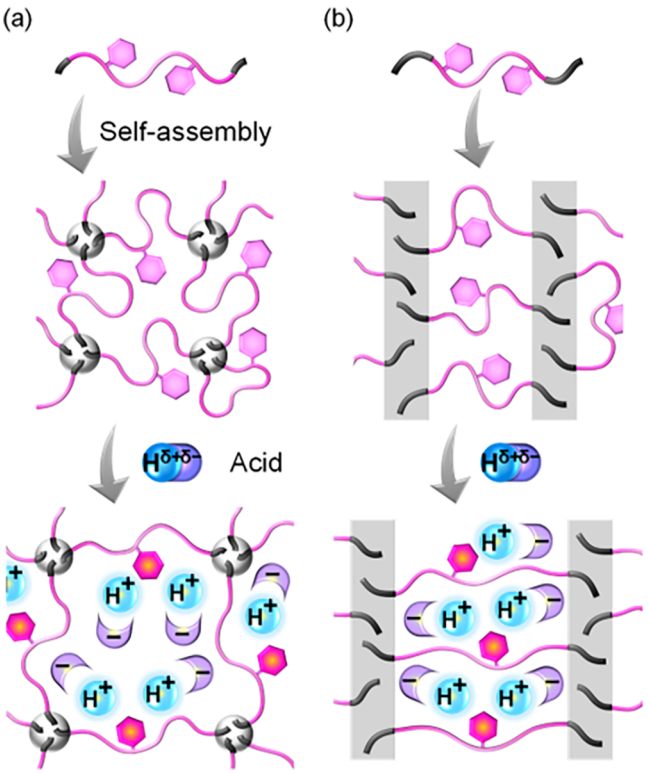

Figure 1. Schematic illustration of the preparation of acid-infiltrated block polymer electrolyte membranes adopting different nanophase-separated structures: (a) Spherical structure. (b) Lamellar structure.

2. EXPERIMENTAL SECTION

2.1. Synthesis and Characterization of Triblock Copolymers. Two S−P−S triblock copolymers with almost the same molecular weight ($M_{n,total}$), but with different ϕ_S values, were synthesized by reversible addition-fragmentation chain transfer (RAFT) polymerization,[50,51] as previously reported.[43] First, styrene purified by passage through an activated alumina column was polymerized by using a bifunctional RAFT agent and 2,2′-azobis(isobutyronitrile) (AIBN) at 130 °C. After polymerization, the product of polystyrene (abbreviated as S) was purified by reprecipitation with methanol. Then, S−P−S was synthesized by polymerizing 4-vinylpyridine by using the S with the RAFT agent residue as a macro-RAFT agent at 80 °C. Two S−P−S with smaller and larger S volume fractions were coded as S−P−S(s) and S−P−S(l), respectively. Molecular characteristics of the two types of S−P−S were determined as previously reported,[43] and Table 1 summarizes molecular characteristics of the two synthesized variants of S−P−S. To estimate the molecular weight distribution of the two S−P−S, gel permeation chromatography was also conducted by using an HPLC system (HPLC pump: Shimadzu LC-20AD; column oven: Shimadzu CTO-20A; RI detector: Shimadzu RID-10; eluent solvent: *N*,*N*-dimethylformamide; flow rate: 1.0 mL min^{-1}) equipped with three TSK gel G4000H$_{HR}$ columns (Tosoh Corp.) at 40 °C (see GPC chromatograms in Figure S1). The degree of polymerization, number-average molecular weight, and composition of the two S−P−S were determined by ^{1}H NMR spectroscopy with an Ascend 500 MHz (Bruker Corp.). The

https://doi.org/10.1021/acsomega.2c06514
ACS Omega 2023, 8, 1121−1130

Table 1. Molecular Characteristics of Neat S−P−S

sample	$M_{n,S}$[a]	$M_{n,total}$[b]	M_w/M_n[c]	φ_S[d]
S−P−S(s)	14,000	180,000	1.6	0.08
S−P−S(l)	33,000	169,000	1.7	0.20

[a]Number-average molecular weight of a precursor S determined by ^{1}H NMR. [b]Total number-average molecular weight of an S−P−S calculated by using a molecular weight of the precursor S and the molar fraction of the S−P−S estimated from ^{1}H NMR. [c]Molecular weight distribution determined by GPC. The molecular weight was calibrated by using polystyrene standards. [d]Volume fraction of S blocks calculated by using the molar fraction of S blocks in S−P−S estimated from ^{1}H NMR and the room-temperature bulk densities of component polymers, i.e., 1.05 g cm^{-3} for S and 1.17 g cm^{-3} for P.[52]

solvent used for spectroscopy was deuterated chloroform. Figure 2 shows the ^{1}H NMR spectra of S−P−S(s) and S−P−S(l), respectively. The integral of the signals originating from three phenyl protons (positions a and b) in the spectrum of S−P−S(l) was obviously larger than in the spectrum of S−P−S(s), indicating that the S fraction of S−P−S(l) was larger than that of S−P−S(s). See also Figure S2 regarding how to determine the molecular weights of S−P−S(s), S−P−S(l), and the precursor S.

2.2. Preparation of S−P−S/H_2SO_4 Membranes. S−P−S/H_2SO_4 membranes were prepared by infiltrating H_2SO_4 into neat S−P−S as previously reported.[43] First, neat S−P−S films were prepared by a solution casting method with pyridine as a solvent, followed by vacuum drying at 50 °C. The neat S−P−S film was immersed into a solution of H_2SO_4 in methanol. Note that no phase transition presumably occurs after infiltration of H_2SO_4 because methanol dissolves P and H_2SO_4 but does not dissolve S. After slowly evaporating the methanol from the solution at 50 °C for 12 h, methanol was added again to homogeneously infiltrate the acid, followed by solution casting at 50 °C for 36 h and vacuum drying at 50 °C for 24 h. The weight content of H_2SO_4 in the S−P−S/H_2SO_4 PEMs ranged from 50 to 80 wt %. S−P−S/H_2SO_4 membranes with less than 50 wt % H_2SO_4 were not prepared because conductivity values of the membranes with less than 50 wt % H_2SO_4 are assumed to be very low under non-humidification according to previous reports.[42,43] For S−P−S(l)/H_2SO_4 with 80 wt % H_2SO_4, all the H_2SO_4 used for membrane preparation cannot be infiltrated in S−P−S(l). This is attributed to both the smaller fraction of H_2SO_4-retaining P of S−P−S(l) than that of S−P−S(s) and the larger interfacial area between the S phase and the P/H_2SO_4 mixed phase in lamellae-forming S−P−S(l) than that of sphere-forming S−P−S(s), where S and H_2SO_4 contact each other. Probably due to such reasons, the easier leaching of H_2SO_4 from S−P−S(l)/H_2SO_4 than S−P−S(s)/H_2SO_4 was observed. The homogeneous PEMs prepared are coded as S−P−S(X)/H_2SO_4(w_{H2SO4}), where X is s or l, and w_{H2SO4} represents the weight percent of H_2SO_4 in the PEM. The molar ratio of H_2SO_4 to a pyridyl group in S−P−S, termed the acid doping level (ADL), can be calculated from eq 1:

$$\mathrm{ADL} = \frac{n_{H2SO4}}{n_P} = \frac{w_{H2SO4}/M_{H2SO4}}{w_P/M_{P,monomer}} = \frac{w_{H2SO4}/M_{H2SO4}}{w_{S-P-S}w'_P/M_{P,monomer}} \quad (1)$$

where n_{H2SO4} and M_{H2SO4} are the molar amount and molecular weight (98 g mol^{-1}) of H_2SO_4, respectively, while n_P, w_P, and $M_{P,monomer}$ are the molar amount, weight amount, and molecular weight (105 g mol^{-1}), respectively, of the 4-vinylpyridine monomer unit in the PEM. The values w_{S-P-S} and w'_P are the weight fraction of S−P−S in the PEMs and weight fraction of P in neat S−P−S, respectively.

2.3. Measurements. Transmission electron microscopy (TEM) observation was carried out for the two types of neat S−P−S. The sample specimen of neat S−P−S was embedded into epoxy resin, followed by preparation of ultrathin microtome sections with a thickness of ∼80 nm in a wet condition. The sections were stained with iodine (I_2) vapor at 50 °C for 50 min. The instrument used for TEM observation was JEM-2100 Plus (JEOL Ltd.), and the acceleration voltage was 200 kV. Note that TEM observation for PEMs infiltrated with H_2SO_4 was not performed because highly acidic H_2SO_4 can damage the TEM instrument if H_2SO_4 is leached out from the PEM during observations.

SAXS measurements were performed at room temperature under an argon atmosphere to acquire quantitative nanostructural information of neat S−P−S and S−P−S/H_2SO_4 membranes. To prevent the membranes from exposure to an air atmosphere, hard samples were enclosed in a glass capillary with a diameter of 1.5 mm whereas soft samples were sandwiched between Kapton films with a thickness of ∼7.5 μm. The measurements were carried out at room temperature using BL-40B2 of the SPring-8 facility, Hyogo, Japan, at a

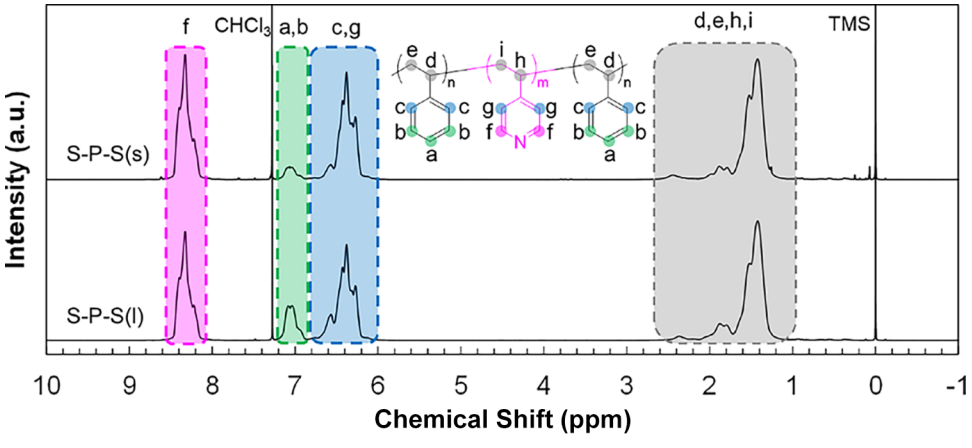

Figure 2. ^{1}H NMR spectra of S−P−S(s) (top) and S−P−S(l) (bottom).

https://doi.org/10.1021/acsomega.2c06514
ACS Omega 2023, 8, 1121−1130

wavelength of 0.15 nm[53,54] and a camera length of 6.25 m with the Pilatus 2M detector.

Tensile tests for the strip-shaped PEMs with a dimension of 20 mm × 4 mm × 0.5 mm were carried out with an Autograph AGS-X (Shimadzu) equipped with a 50 N load cell and 50 N pneumatic flat grips. The tests were conducted at an initial between-jigs distance of about 10 mm with an initial strain rate of approximately 0.10 s^{-1} (an elongation rate of 1.0 mm s^{-1}) at room temperature.[55,56]

The conductivities of the PEMs were determined as previously reported[42,43] by alternating current impedance spectroscopy with a potentio/galvanostat VSP-300 (BioLogic Science Instruments) in the frequency range of 1×10^0 to 7×10^6 Hz at a signal amplitude of 50 mV by using a two-probe method. A test cell was prepared by fixing the distance (l) between the platinum electrodes at 7 mm and using the test specimen with sectional area (A) of ∼2 mm^2 (see also the schematic of the impedance spectroscopy setup in Figure S4). The temperature and humidity were controlled in the benchtop-type environmental chamber SH-242 (ESPEC Corp.) within a temperature range of 20−95 °C below the T_g of polystyrene (∼100 °C) at no humidification, where the humidity in the chamber at all temperatures was determined to be close to 0 %RH by the thermohygrometer Testo 645 (Testo SE & Co. KgaA). To estimate the conductivity (σ_{DC}) by using eq 2, a bulk resistance (R) of the PEMs was evaluated by reading the extrapolated value of the plot on the horizontal axis (nonzero Z' intercept in the Nyquist plot[39,43,57]), where Z' is the real part of the complex impedance $Z = Z' - iZ''$ (see also the Nyquist plots of S−P−S/H_2SO_4 membranes in Figure S5).

$$\sigma_{DC} = \frac{l}{AR} \tag{2}$$

3. RESULTS AND DISCUSSION

3.1. Nanophase-Separated Structure of Neat S−P−S and PEMs. Typical TEM images of neat S−P−S(s) and neat S−P−S(l) are displayed in Figure 3a,b, respectively, where the

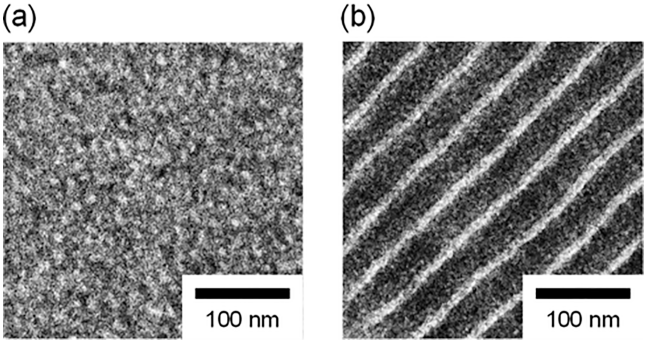

Figure 3. TEM images of (a) neat S−P−S(s) and (b) neat S−P−S(l).

S phase appears brighter while the P phase looks darker because of I_2 vapor staining.[58,59] A brighter spherical S phase with discontinuity in the darker P phase as a continuous matrix was observed in the TEM image of neat S−P−S(s). Based on the TEM image, domain spacing (D) of neat S−P−S(s) was estimated to be ∼25 nm. On the other hand, neat S−P−S(l) showed a lamellar structure with D ∼ 45 nm composed of a thin S-layered phase and a thick P-layered phase. The lamellar structure was formed in neat S−P−S(l) in spite of a relatively small φ_S, probably due to the relatively large molecular weight distribution of S−P−S(l) (M_w/M_n = 1.7).[60−62]

SAXS measurements were also carried out to investigate quantitative nanostructural information of the two neat S−P−S. SAXS profiles of neat S−P−S(s) and neat S−P−S(l) are shown in Figure 4a,b, respectively. The profile of S−P−S(s) at

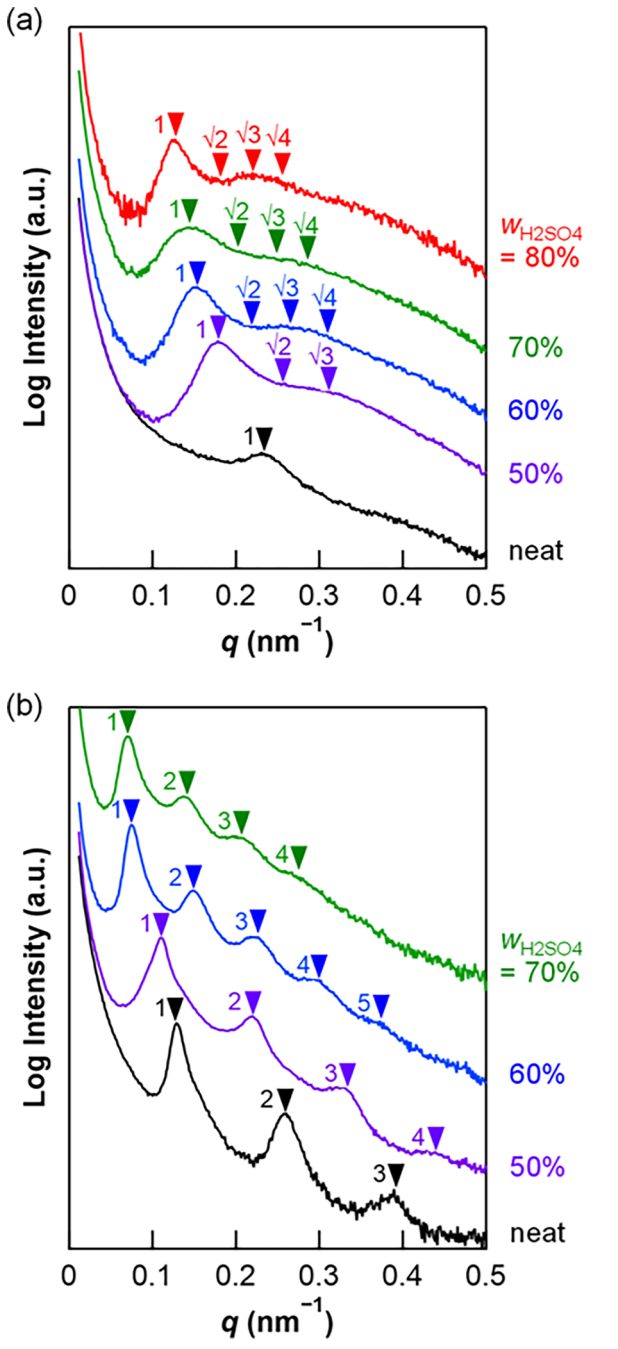

Figure 4. SAXS profiles of (a) S−P−S(s)/H_2SO_4 and (b) S−P−S(l)/H_2SO_4.

the bottom of Figure 4a (profile with black lines) showed a peak at a scattering vector q (= $4\pi \sin \theta/\lambda$) of 0.23 nm^{-1}, where λ and 2θ are the wavelength of X-rays and the scattering angle, respectively. Taking account also of both the TEM results of S−P−S(s) and a general self-assembly manner of block polymers, the S spherical domains in neat S−P−S(s) are assumed to be packed in a bcc lattice,[63,64] and D of neat S−P−

https://doi.org/10.1021/acsomega.2c06514
ACS Omega 2023, 8, 1121−1130

Table 2. Properties of Neat S−P−S and S−P−S/H_2SO_4 Membranes

sample	w_{H2SO4}[a] (wt %)	ADL[b]	D[c] (nm)	E_Y[d] (MPa)	σ_{max}[e] (MPa)	ε_b[f] (%)	T_g[g] (°C)	$\sigma_{DC,95\ °C}$[h] (S cm^{-1})
neat S−P−S(s)	0	0	24	n.d.[i]	n.d.[i]	n.d.[i]	138	n.d.[i]
S−P−S(s)/H_2SO_4(50)	50	1.2	30	12	1.7	58	52	1.5×10^{-4}
S−P−S(s)/H_2SO_4(60)	60	1.7	35	0.60	0.43	580	−61	0.012
S−P−S(s)/H_2SO_4(70)	70	2.7	38	0.17	0.18	510	−75	0.062
S−P−S(s)/H_2SO_4(80)	80	4.6	45	0.039	0.032	210	−80	0.14
neat S−P−S(l)	0	0	49	n.d.[i]	n.d.[i]	n.d.[i]	141	n.d.[i]
S−P−S(l)/H_2SO_4(50)	50	1.3	57	43	2.7	47	31	0.0011
S−P−S(l)/H_2SO_4(60)	60	2.0	84	33	1.4	120	−60	0.039
S−P−S(l)/H_2SO_4(70)	70	3.1	91	4.2	0.75	99	−75	0.061

[a]Weight fraction of H_2SO_4 in a sample. [b]Acid doping level calculated from eq 1. [c]Domain-spacing estimated from SAXS (see also Table S1). [d]Young's modulus estimated from the slope from the strain range from 1 to 3%. [e]Tensile strength. [f]Elongation at break. [g]Glass transition temperature of the P or P/H_2SO_4 mixed phase determined by DSC (Figure S3). Note that T_g of the S phase was not clearly observed by DSC due to the small volume fraction of S in S−P−S/H_2SO_4. However, T_g derived from S should exist because the S phase was observed by TEM and SAXS. [h]Conductivity at 95 °C under non-humidification. [i]Not determined.

S(s) is estimated to be ∼24 nm by using the first peak q position (q_1) of the SAXS profile and the eq $D = (3/4)^{1/2} \times 2\pi/q_1$,[59] which roughly agreed with the TEM result (see also q_1 and D values in Table S1). Note that the second peak was not clearly observed in the profile of neat S−P−S(s), indicating spherical domains were arranged in a poorly ordered manner. On the other hand, the SAXS profile of neat S−P−S(l) at the bottom of Figure 4b clearly showed integer-order peaks relative to the first peak ($q_1 = 0.13$ nm^{-1}), indicating formation of the lamellar structure with D (= $2\pi/q_1$[59]) ∼49 nm in S−P−S(l). This result was also consistent with D estimated from the TEM image of neat S−P−S(l).

SAXS measurements for S−P−S/H_2SO_4 membranes were also conducted to acquire information about the nanostructures of S−P−S infiltrated with H_2SO_4. Figure 4a shows SAXS profiles of S−P−S(s)/H_2SO_4 membranes as well as the profile of neat S−P−S(s). In a profile of the S−P−S(s)/H_2SO_4 membrane with 50 wt % H_2SO_4, scattering intensities at $\sqrt{2}q_1$ and $\sqrt{3}q_1$ were relatively strong, compared with the weaker intensities in a profile of neat S−P−S(s). This outcome may be attributed to improved ordering of the spherical domain packing resulting from stronger segregation between hydrophobic S and hydrophilic P/H_2SO_4 mixed phases than between S and P phases.[53] Furthermore, as the amount of H_2SO_4 in S−P−S(s)/H_2SO_4 membranes increased, the first peak also shifted to lower q, while the profile pattern was mostly retained (see also q_1 values in Table S1). These results indicated that domain spacing (D) became larger without morphology transition by selectively infiltrating H_2SO_4 into the P matrix phase (see also D values in Table S1). Similarly, all the profiles of S−P−S(l)/H_2SO_4 membranes in Figure 4b showed the integer-order peak as neat S−P−S(l), indicating that the lamellar structure remained in the S−P−S(l)/H_2SO_4 membranes even in the presence of infiltrating H_2SO_4. In addition to S−P−S(s)/H_2SO_4, the first peak of S−P−S(l)/H_2SO_4 membranes also shifted to the lower q side with the addition of more Sa to the neat S−P−S(l). Table 2 summarizes D of S−P−S/H_2SO_4 membranes estimated from the SAXS profiles, and D is plotted against w_{H2SO4} in Figure 5. For both S−P−S(s)/H_2SO_4 and S−P−S(l)/H_2SO_4, D seems to depend more strongly on w_{H2SO4} in the range from 50 to 80 wt % compared with the range below 50 wt %. This dependence is probably due to acid−base complexation[65] between H_2SO_4 and the pyridyl group in the P/H_2SO_4 mixed phase. At the ADL below unity or w_{H2SO4} below approximately 50 wt %, P

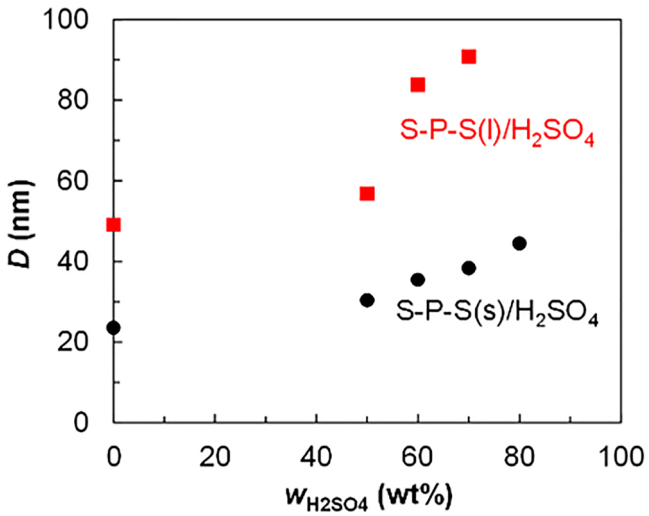

Figure 5. Domain spacing of S−P−S/H_2SO_4 as a function of w_{H2SO4}.

block chains largely shrink by strong ionic interactions attributed to acid−base complexation. On the other hand, when the ADL was larger than unity, the P chains were swollen because an excess amount of H_2SO_4 behaves like a plasticizer, leading to a rapid D increase. In addition, the D of S−P−S(l)/H_2SO_4 was more strongly dependent on w_{H2SO4} compared with D of S−P−S(s)/H_2SO_4. This result is probably due to the difference in the nanostructure dimensionality and the swelling behavior. Note that the effect of one-dimensional swelling of polymer chains in S−P−S(l)/H_2SO_4 resulting in an increase in D was larger than that of three-dimensional swelling observed in S−P−S(s)/H_2SO_4.

3.2. Mechanical Properties of S−P−S/H_2SO_4 Membranes. To investigate the effect of the phase-separated structure of the block polymer-based PEMs on the mechanical properties, tensile tests for S−P−S/H_2SO_4 membranes were performed. Figure 6a,b shows tensile stress−strain curves of a series of S−P−S(s)/H_2SO_4 and S−P−S(l)/H_2SO_4 membranes, respectively, when measured at room temperature. Table 2 also summarizes Young's modulus (E_Y), tensile strength (σ_{max}), and elongation at break (ε_b) of the S−P−S/H_2SO_4 membranes. The E_Y, σ_{max}, and ε_b values of the S−P−S(s)/H_2SO_4(50) membrane were 12 MPa, 1.7 MPa, and 58%, respectively, indicating a brittle plastic-like behavior.[66] In contrast, the S−P−S(s)/H_2SO_4(60) membrane exhibited a

https://doi.org/10.1021/acsomega.2c06514
ACS Omega 2023, 8, 1121−1130

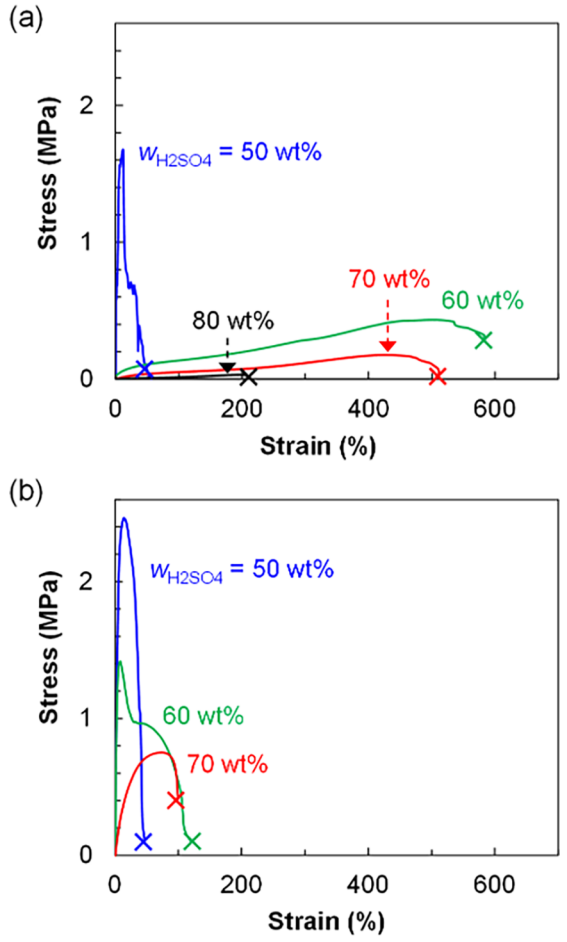

Figure 6. Tensile stress−strain curves of a series of (a) S−P−S(s)/H_2SO_4 and (b) S−P−S(l)/H_2SO_4 membranes.

lower E_Y (0.60 MPa) and σ_{max} (0.43 MPa) but a larger ε_b (580%), which indicated that the membrane shows an elastomeric behavior.[55] As the H_2SO_4 content increased further, E_Y, σ_{max}, and even ε_b decreased (Table 2). At w_{H2SO4} = 50 wt %, that is, ADL is close to 1, T_g of the P/H_2SO_4 mixed phase was much higher than room temperature due to formation of a hard acid−base complex of H_2SO_4 and the pyridyl group. Since T_g of the S phase in S−P−S(s)/H_2SO_4(50) was approximately 100 °C, also higher than room temperature, the S−P−S(s)/H_2SO_4 (50) membrane behaved like a brittle plastic at room temperature. On the other hand, when w_{H2SO4} exceeded 60 wt %, T_g of the P/H_2SO_4 mixed phase became lower than room temperature by the presence of an excessive amount of H_2SO_4 serving as a plasticizer in the mixed phase, causing the membranes to behave like an elastomer.

The S−P−S(l)/H_2SO_4(50) membrane also exhibited a brittle plastic-like behavior similar to the S−P−S(s)/H_2SO_4(50) membrane. Similarly, as w_{H2SO4} increased, S−P−S(l)/H_2SO_4 membranes also behaved like an elastomer; namely, E_Y and σ_{max} of S−P−S(l)/H_2SO_4 membranes decreased and its ε_b increased as well as the S−P−S(s)/H_2SO_4 membranes (Table 2). However, it should also be noted that the elastomer-like S−P−S(l)/H_2SO_4 exhibited much better mechanical strength compared with the elastomer-like S−P−S(s)/H_2SO_4 membranes with the same w_{H2SO4}. For example, E_Y and σ_{max} of S−P−S(l)/H_2SO_4(70) were 25 times and 4.2 times, respectively, higher than the same properties of the S−P−S(s)/H_2SO_4(70) membrane. Since the morphology of the hard S phase in S−P−S(l)/H_2SO_4 membranes is a planar layer with a higher degree of continuity while that of the hard S phase in S−P−S(s)/H_2SO_4 membranes is a discontinuous sphere, the continuity of the hard S-layered phase in S−P−S(l)/H_2SO_4 membranes probably contributes greatly to the higher mechanical strength. Therefore, if a hard three-dimensionally continuous S phase such as gyroid phase is formed in the membrane, such a membrane can exhibit higher mechanical strength than that of lamella-forming S−P−S(l)/H_2SO_4 membranes with a two-dimensionally continuous S phase.

3.3. Conductivity of S−P−S/H_2SO_4 Membranes under Non-Humidification. Figure 7 shows the plot of σ_{DC} for S−P−S/H_2SO_4 membranes against the reciprocal of the absolute temperature (T) (see also the Nyquist plots for S−P−S/H_2SO_4 membranes in Figure S5). The σ_{DC} of the S−P−S(s)/H_2SO_4 membranes under non-humidification increased with

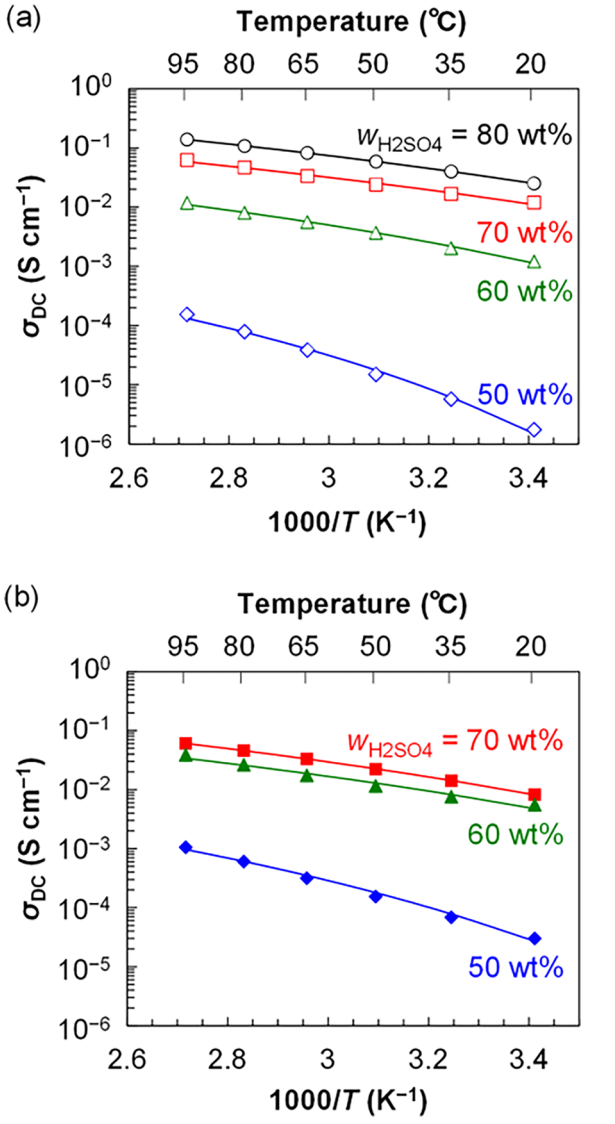

Figure 7. Temperature dependence of conductivity of a series of (a) S−P−S(s)/H_2SO_4 and (b) S−P−S(l)/H_2SO_4 membranes under non-humidification. Solid lines are fits by the VFT equation.

https://doi.org/10.1021/acsomega.2c06514
ACS Omega 2023, 8, 1121−1130

increasing temperature for all samples. The σ_{DC} of S−P−S(s)/H_2SO_4 membranes was also fitted by the Vogel−Fulcher−Tammann (VFT) equation (eq S1), which is useful for fitting σ_{DC} influenced by T_g[39] (see also Table S2 and Figure S6 for the fitting parameters). The σ_{DC} of the S−P−S(s)/H_2SO_4(50) membrane exhibited a low σ_{DC} of 1.5×10^{-4} S cm^{-1} under non-humidification even at the highest temperature of 95 °C adopted in this study, while the S−P−S(s)/H_2SO_4(60) membrane showed a moderately high σ_{DC} of 1.2×10^{-2} S cm^{-1}, two orders of magnitude larger at the same temperature under dry conditions. As the H_2SO_4 content increased further, membranes such as S−P−S(s)/H_2SO_4(70) and S−P−S(s)/H_2SO_4(80) exhibited much higher values of σ_{DC} of 6.2×10^{-2} and 1.4×10^{-1} S cm^{-1}, respectively. These results are consistent with our previous study.[42,43] Similar to S−P−S(s)/H_2SO_4 membranes, the σ_{DC} values of S−P−S(l)/H_2SO_4 membranes with the lamellar structure under non-humidification also increased with increasing w_{H2SO4}, but notably, the absolute value of σ_{DC} of S−P−S(l)/H_2SO_4 was generally higher than that of S−P−S(s)/H_2SO_4 under non-humidification when w_{H2SO4} was the same. Namely, the S−P−S(l)/H_2SO_4(50) membrane exhibited the σ_{DC} of 1.6×10^{-3} S cm^{-1} under non-humidification, a conductivity that is one order of magnitude higher than that of the S−P−S(s)/H_2SO_4(50) membrane at 95 °C (1.5×10^{-4} S cm^{-1}). The σ_{DC} of S−P−S(l)/H_2SO_4(60) was 4.6×10^{-2} S cm^{-1}, a conductivity approximately three times higher than that of S−P−S(s)/H_2SO_4(60) at the same temperature (1.2×10^{-2} S cm^{-1}). The σ_{DC} of S−P−S(l)/H_2SO_4(70) was 6.1×10^{-2} S cm^{-1}, which is comparable to that of S−P−S(s)/H_2SO_4(70).

To compare the σ_{DC} of the S−P−S(l)/H_2SO_4 membranes with that of S−P−S(s)/H_2SO_4 when w_{H2SO4} is the same, the σ_{DC} at 95 °C under non-humidification was plotted against w_{H2SO4} (Figure 8a). The σ_{DC} values are summarized in Table 2. The conductivity of both S−P−S(s)/H_2SO_4 and S−P−S(l)/H_2SO_4 increased as w_{H2SO4} increased, while the conductivity of S−P−S(l)/H_2SO_4 was higher than or comparable to that of S−P−S(s)/H_2SO_4 with the same w_{H2SO4}. Taking acid−base complexation between H_2SO_4 and the pyridyl group of S−P−S in the membranes into account, the molar ratio of acid to base, i.e., ADL, should directly affect the σ_{DC} under non-humidification because the number of protons released from free H_2SO_4 is strongly dependent on acid−base complexation, which consumes the free protons.

The relationship between the σ_{DC} under non-humidification and ADL of S−P−S/H_2SO_4 is exhibited in the plot in Figure 8b. Surprisingly, data points of σ_{DC} for both S−P−S(s)/H_2SO_4 and S−P−S(l)/H_2SO_4 membranes under non-humidification followed almost the same curve. In other words, the conductivity dependence for ADL is almost the same for S−P−S(s)/H_2SO_4 and S−P−S(l)/H_2SO_4, and the σ_{DC} of the S−P−S/H_2SO_4 membranes was greatly influenced by the acid/base stoichiometry associated with acid−base complex formation rather than the nanophase-separated structure adopted in the membranes. Although the experimental data was not measured for the region of ADL <1 in this study, the σ_{DC} at ADL <1 is expected to be very low, below 10^{-4} S cm^{-1} according to our previous studies.[42,43] In the region of ADL >1, the membranes exhibit the σ_{DC} of 10^{-4} S cm^{-1} or higher, and the larger the ADL, the higher the σ_{DC}. For example, the σ_{DC} was 0.039 S cm^{-1} at ADL = 2.0, but when ADL >2, the degree of increase in conductivity decreased.

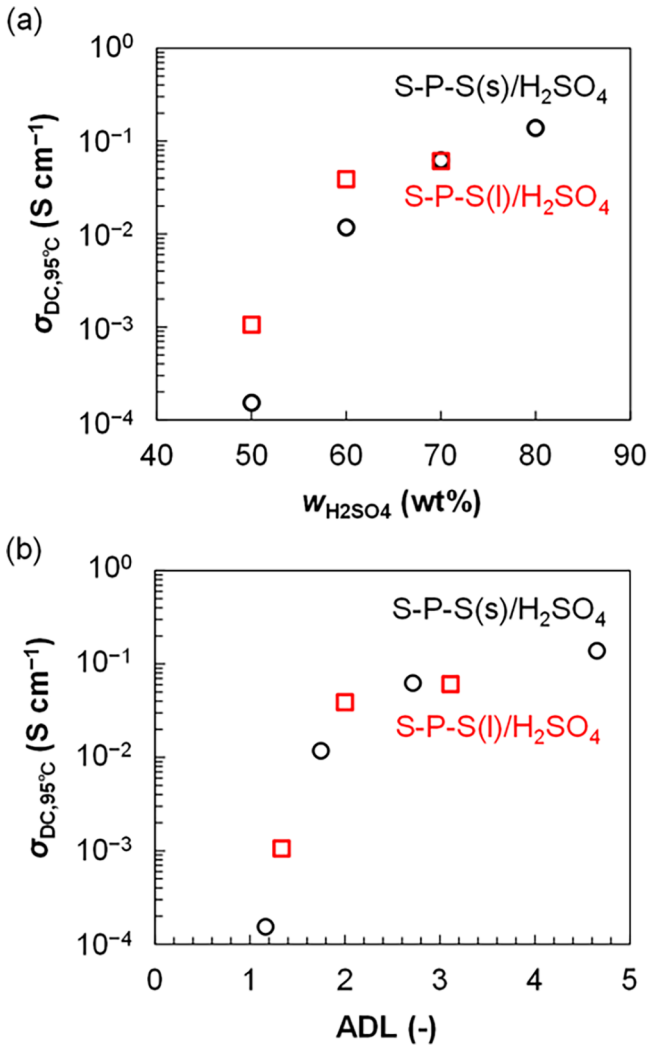

Figure 8. Conductivity at 95 °C under non-humidification for a series of S−P−S/H_2SO_4 membranes against (a) w_{H2SO4} and (b) ADL.

The very low σ_{DC} in the region of ADL <1 may reflect the few free protons directly contributing to conductivity, because almost all free H_2SO_4 in the membranes contributed to the formation of rigid ionic acid−base complexes consisting of a hydrogen sulfate anion and the protic pyridinium cation (Figure 9a). When the ADL exceeds unity, the excess H_2SO_4 not used for acid−base complex formation is mixed with rigid acid−base complexes as a plasticizer, and free protons promoting proton transport are generated by ionization of free H_2SO_4, attaining proton conduciveness of the membranes (Figure 9b). As the ADL became larger, the ionic interactions that arise in the acid−base complexes are further weakened and the acid−base complexes become softer due to the infiltration of more excess H_2SO_4 as a plasticizer (Figure 9c). Moreover, the absolute number of free protons generated by ionization of excess H_2SO_4 also increases, inducing the higher conductivity of the membranes. Note that the degree of the increase in the fraction of free protons declines in the region of ADL > 2, resulting in the gradual increase in σ_{DC}. In short, since the σ_{DC} dependence on ADL is almost the same for S−P−S(l)/H_2SO_4 and S−P−S(s)/H_2SO_4, S−P−S(l)/H_2SO_4, which has a smaller fraction of P, exhibits comparable or higher σ_{DC} than that of S-P-S(s)/H_2SO_4, even when w_{H2SO4} is the same for both membranes.

https://doi.org/10.1021/acsomega.2c06514
ACS Omega 2023, 8, 1121−1130

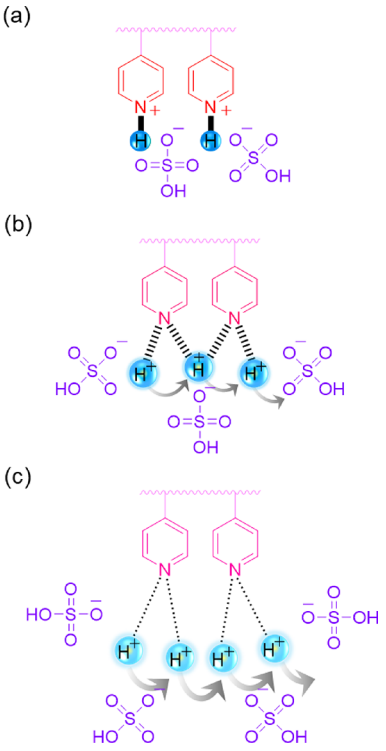

Figure 9. Schematic illustration of H_2SO_4 and pyridyl groups in S−P−S/H_2SO_4 at the molecular level for (a) ADL <1, (b) 1< ADL <2, and (c) ADL >2.

4. CONCLUSIONS

We investigated the effects of the nanophase-separated structure on the mechanical properties and proton conductivity of acid-infiltrated block polymer electrolyte membranes adopting a spherical or lamellar nanophase-separated structure by infiltrating sulfuric acid into S−P−S triblock copolymers. SAXS measurements revealed that no morphology transition occurred even after the infiltration of H_2SO_4 into neat S−P−S films. S−P−S(l)/H_2SO_4 membranes with a continuous hard S phase generally exhibited higher tensile strength than S−P−S(s)/H_2SO_4 membranes forming a spherical structure, even if the same amount of H_2SO_4 was infiltrated into each type of neat S−P−S film. Meanwhile, the conductivities of S−P−S(l)/H_2SO_4 membranes under non-humidification were higher or comparable to those of S−P−S(s)/H_2SO_4 membranes with the same w_{H2SO4}. This outcome reflects the strong dependence of the σ_{DC} of the S−P−S/H_2SO_4 membranes on ADL, i.e., the stoichiometric ratio of acid to base, rather than on the nanophase-separated structure adopted in the membranes. In other words, there are more free molecules of H_2SO_4 that are not consumed for acid−base complexation, which can then release more free protons in S−P−S(l)/H_2SO_4 compared to S−P−S(s)/H_2SO_4 with the same weight fraction of H_2SO_4. This feature originates from the molecular characteristics of the two types of S−P−S, i.e., the difference in the fraction of the basic P block in S−P−S. Although the infiltrated acid is easily dissolved out in water from the S−P−S/H_2SO_4 membranes if the membranes are put into water, the S−P−S/H_2SO_4 membranes exhibit good conductivities even under non-humidification unlike the Nafion membrane; therefore, the S−P−S/H_2SO_4 membranes still have a high potential for application into PEFCs that can generate electricity even under non-humidification, if dissolving out of acid into water can be suppressed. The findings obtained in this study will help to design high-performance PEMs for development of next-generation fuel cells.

■ ASSOCIATED CONTENT

Supporting Information

The Supporting Information is available free of charge at https://pubs.acs.org/doi/10.1021/acsomega.2c06514.

GPC chromatograms of S−P−S(s) and S−P−S(l); ^{1}H NMR spectra of S−P−S(s), S−P−S(l), and precursor S; DSC thermograms for a series of S−P−S(s)/H_2SO_4 and S−P−S(l)/H_2SO_4 membranes; the impedance spectroscopy setup; the q_1 and D of the SAXS profile; Nyquist plots of S−P−S/H_2SO_4 membranes; and VFT fitting (Figures S1−S6 and Tables S1−S2) (PDF)

■ AUTHOR INFORMATION

Corresponding Author

Atsushi Noro − *Department of Molecular & Macromolecular Chemistry, Graduate School of Engineering, Nagoya University, Nagoya 464-8603, Japan; Research Center for Net-Zero Carbon Society, Institutes of Innovation for Future Society, Nagoya University, Nagoya 464-8601, Japan;* orcid.org/0000-0002-3336-763X; Email: noro@nagoya-u.jp

Authors

Takato Kajita − *Department of Molecular & Macromolecular Chemistry, Graduate School of Engineering, Nagoya University, Nagoya 464-8603, Japan;* orcid.org/0000-0002-5146-1953

Haruka Tanaka − *Department of Molecular & Macromolecular Chemistry, Graduate School of Engineering, Nagoya University, Nagoya 464-8603, Japan*

Yumiko Ohtsuka − *Department of Molecular & Macromolecular Chemistry, Graduate School of Engineering, Nagoya University, Nagoya 464-8603, Japan*

Tsuyoshi Orido − *Department of Molecular & Macromolecular Chemistry, Graduate School of Engineering, Nagoya University, Nagoya 464-8603, Japan*

Atsushi Takano − *Department of Molecular & Macromolecular Chemistry, Graduate School of Engineering, Nagoya University, Nagoya 464-8603, Japan;* orcid.org/0000-0002-5188-5166

Hiroyuki Iwamoto − *Japan Synchrotron Radiation Research Institute (JASRI), Sayo-gun, Hyogo 679-5198, Japan*

Albert Mufundirwa − *Japan Synchrotron Radiation Research Institute (JASRI), Sayo-gun, Hyogo 679-5198, Japan*

Hideto Imai − *NISSAN ARC LTD., Yokosuka, Kanagawa 237-0061, Japan;* Present Address: Fuel Cell Cutting-Edge Research Center Technology Research Association, 2-3-26 Aomi, Koto-ku, Tokyo 135-0064, Japan; orcid.org/0000-0002-9434-1492

Complete contact information is available at: https://pubs.acs.org/10.1021/acsomega.2c06514

Author Contributions

The manuscript was written through contributions of all authors. A.N. conceived the original idea and designed the study with T.K. T.K. carried out the tensile tests and DSC measurements. H.T. and Y.O. performed polymer synthesis, sample preparation, and conductivity measurements. T.O. and

https://doi.org/10.1021/acsomega.2c06514
ACS Omega 2023, 8, 1121−1130

A.T. conducted TEM observation. H.Iw., A.M., and H.Im. carried out SAXS measurements. A.N. and T.K. analyzed the data and co-wrote the paper with input from all authors. All authors have given approval to the final version of the manuscript.

Notes

The authors declare no competing financial interest.

■ ACKNOWLEDGMENTS

The authors thank Dr. Masaki Ando, Dr. Naoki Nakamura, and Mr. Seiji Sano at Toyota Motor Corporation for their kind advice on preparation and evaluation of proton-conductive polymer electrolyte membranes. This work was supported through a project (JPN P20003) subsidized by the New Energy and Industrial Technology Development Organization (NEDO) and KAKENHI grant numbers (21 K05197 (A.N.)) from JSPS, Japan. This research was technically supported by NEDO FC-Platform. The synchrotron experiment was performed at BL40B2 at SPring-8 under approval of the Japan Synchrotron Radiation Research Institute (JASRI) with proposal no. 2021A2054.

■ REFERENCES

(1) O'Hayre, R.; Cha, S.-W.; Colella, W.; Prinz, F. B.*Fuel Cell Fundamentals*; John Wiley & Sons, Inc.: Hoboken, NJ, USA, 2016. DOI: 10.1002/9781119191766.

(2) Dicks, A. L.; Rand, D. A. J.*Fuel Cell Systems Explained*; John Wiley & Sons, Ltd.: West Sussex, PO19 8SQ, UK, 2018. DOI: 10.1002/9781118706992.

(3) Springer, T. E.; Zawodzinski, T. A.; Gottesfeld, S. Polymer Electrolyte Fuel Cell Model. *J. Electrochem. Soc.* **1991**, *138*, 2334−2342.

(4) Zhang, H.; Shen, P. K. Recent Development of Polymer Electrolyte Membranes for Fuel Cells. *Chem. Rev.* **2012**, *112*, 2780−2832.

(5) Wang, Y.; Ruiz Diaz, D. F.; Chen, K. S.; Wang, Z.; Adroher, X. C. Materials, Technological Status, and Fundamentals of PEM Fuel Cells − A Review. *Mater. Today* **2020**, *32*, 178−203.

(6) Jiao, K.; Xuan, J.; Du, Q.; Bao, Z.; Xie, B.; Wang, B.; Zhao, Y.; Fan, L.; Wang, H.; Hou, Z.; Huo, S.; Brandon, N. P.; Yin, Y.; Guiver, M. D. Designing the next Generation of Proton-Exchange Membrane Fuel Cells. *Nature* **2021**, *595*, 361−369.

(7) Onovwiona, H. I.; Ugursal, V. I. Residential Cogeneration Systems: Review of the Current Technology. *Renewable Sustainable Energy Rev.* **2006**, *10*, 389−431.

(8) Mauritz, K. A.; Moore, R. B. State of Understanding of Nafion. *Chem. Rev.* **2004**, *104*, 4535−4586.

(9) Karimi, M. B.; Mohammadi, F.; Hooshyari, K. Recent Approaches to Improve Nafion Performance for Fuel Cell Applications: A Review. *Int. J. Hydrogen Energy* **2019**, *44*, 28919−28938.

(10) Peron, J.; Mani, A.; Zhao, X.; Edwards, D.; Adachi, M.; Soboleva, T.; Shi, Z.; Xie, Z.; Navessin, T.; Holdcroft, S. Properties of Nafion® NR-211 Membranes for PEMFCs. *J. Membr. Sci.* **2010**, *356*, 44−51.

(11) Gierke, T. D.; Munn, G. E.; Wilson, F. C. The Morphology in Nafion Perfluorinated Membrane Products, as Determined by Wide- and Small-Angle x-Ray Studies. *J. Polym. Sci. Polym. Phys. Ed.* **1981**, *19*, 1687−1704.

(12) Schmidt-Rohr, K.; Chen, Q. Parallel Cylindrical Water Nanochannels in Nafion Fuel-Cell Membranes. *Nat. Mater.* **2008**, *7*, 75−83.

(13) Wainright, J. S.; Wang, J.-T.; Weng, D.; Savinell, R. F.; Litt, M. Acid-Doped Polybenzimidazoles: A New Polymer Electrolyte. *J. Electrochem. Soc.* **1995**, *142*, L121−L123.

(14) Bouchet, R.; Siebert, E. Proton Conduction in Acid Doped Polybenzimidazole. *Solid State Ionics* **1999**, *118*, 287−299.

(15) Schuster, M. F. H.; Meyer, W. H. Anhydrous Proton-Conducting Polymers. *Annu. Rev. Mater. Res.* **2003**, *33*, 233−261.

(16) Xiao, L.; Zhang, H.; Scanlon, E.; Ramanathan, L. S.; Choe, E.-W.; Rogers, D.; Apple, T.; Benicewicz, B. C. High-Temperature Polybenzimidazole Fuel Cell Membranes via a Sol−Gel Process. *Chem. Mater.* **2005**, *17*, 5328−5333.

(17) Ye, H.; Huang, J.; Xu, J. J.; Kodiweera, N. K. A. C.; Jayakody, J. R. P.; Greenbaum, S. G. New Membranes Based on Ionic Liquids for PEM Fuel Cells at Elevated Temperatures. *J. Power Sources* **2008**, *178*, 651−660.

(18) Bureekaew, S.; Horike, S.; Higuchi, M.; Mizuno, M.; Kawamura, T.; Tanaka, D.; Yanai, N.; Kitagawa, S. One-Dimensional Imidazole Aggregate in Aluminium Porous Coordination Polymers with High Proton Conductivity. *Nat. Mater.* **2009**, *8*, 831−836.

(19) van de Ven, E.; Chairuna, A.; Merle, G.; Benito, S. P.; Borneman, Z.; Nijmeijer, K. Ionic Liquid Doped Polybenzimidazole Membranes for High Temperature Proton Exchange Membrane Fuel Cell Applications. *J. Power Sources* **2013**, *222*, 202−209.

(20) Lee, S.-Y.; Ogawa, A.; Kanno, M.; Nakamoto, H.; Yasuda, T.; Watanabe, M. Nonhumidified Intermediate Temperature Fuel Cells Using Protic Ionic Liquids. *J. Am. Chem. Soc.* **2010**, *132*, 9764−9773.

(21) Song, M.-K.; Li, H.; Li, J.; Zhao, D.; Wang, J.; Liu, M. Tetrazole-Based, Anhydrous Proton Exchange Membranes for Fuel Cells. *Adv. Mater.* **2014**, *26*, 1277−1282.

(22) Lee, K.-S.; Spendelow, J. S.; Choe, Y.-K.; Fujimoto, C.; Kim, Y. S. An Operationally Flexible Fuel Cell Based on Quaternary Ammonium-Biphosphate Ion Pairs. *Nat. Energy* **2016**, *1*, 16120.

(23) Liu, F.; Wang, S.; Chen, H.; Li, J.; Tian, X.; Wang, X.; Mao, T.; Xu, J.; Wang, Z. Cross-Linkable Polymeric Ionic Liquid Improve Phosphoric Acid Retention and Long-Term Conductivity Stability in Polybenzimidazole Based PEMs. *ACS Sustainable Chem. Eng.* **2018**, *6*, 16352−16362.

(24) Li, X.; Ma, H.; Wang, P.; Liu, Z.; Peng, J.; Hu, W.; Jiang, Z.; Liu, B.; Guiver, M. D. Highly Conductive and Mechanically Stable Imidazole-Rich Cross-Linked Networks for High-Temperature Proton Exchange Membrane Fuel Cells. *Chem. Mater.* **2020**, *32*, 1182−1191.

(25) Lee, S.; Seo, K.; Ghorpade, R. V.; Nam, K.-H.; Han, H. High Temperature Anhydrous Proton Exchange Membranes Based on Chemically-Functionalized Titanium/Polybenzimidazole Composites for Fuel Cells. *Mater. Lett.* **2020**, *263*, No. 127167.

(26) Mukhopadhyay, S.; Das, A.; Jana, T.; Das, S. K. Fabricating a MOF Material with Polybenzimidazole into an Efficient Proton Exchange Membrane. *ACS Appl. Energy Mater.* **2020**, *3*, 7964−7977.

(27) Karimi, M. B.; Hooshyari, K.; Salarizadeh, P.; Beydaghi, H.; Ortiz-Martínez, V. M.; Ortiz, A.; Uribe, I. O.; Mohammadi, F. A Comprehensive Review on the Proton Conductivity of Proton Exchange Membranes (PEMs) under Anhydrous Conditions: Proton Conductivity Upper Bound. *Int. J. Hydrogen Energy* **2021**, *46*, 34413−34437.

(28) Atanasov, V.; Lee, A. S.; Park, E. J.; Maurya, S.; Baca, E. D.; Fujimoto, C.; Hibbs, M.; Matanovic, I.; Kerres, J.; Kim, Y. S. Synergistically Integrated Phosphonated Poly(Pentafluorostyrene) for Fuel Cells. *Nat. Mater.* **2021**, *20*, 370−377.

(29) Guo, H.; Li, Z.; Pei, H.; Sun, P.; Zhang, L.; Li, P.; Yin, X. Stable Branched Polybenzimidazole High Temperature Proton Exchange Membrane: Crosslinking and Pentaphosphonic-Acid Doping Lower Fuel Permeability and Enhanced Proton Transport. *J. Membr. Sci.* **2022**, *644*, No. 120092.

(30) Harilal; Bhattacharyya, R.; Shukla, A.; Chandra Ghosh, P.; Jana, T. Rational Design of Microporous Polybenzimidazole Framework for Efficient Proton Exchange Membrane Fuel Cells. *J. Mater. Chem. A* **2022**, *10*, 11074−11091.

(31) Lim, K. H.; Lee, A. S.; Atanasov, V.; Kerres, J.; Park, E. J.; Adhikari, S.; Maurya, S.; Manriquez, L. D.; Jung, J.; Fujimoto, C.; Matanovic, I.; Jankovic, J.; Hu, Z.; Jia, H.; Kim, Y. S. Protonated

Phosphonic Acid Electrodes for High Power Heavy-Duty Vehicle Fuel Cells. *Nat. Energy* **2022**, *7*, 248−259.
(32) Chin, D.-T.; Chang, H. H. On the Conductivity of Phosphoric Acid Electrolyte. *J. Appl. Electrochem.* **1989**, *19*, 95−99.
(33) Angell, C. A.; Byrne, N.; Belieres, J.-P. Parallel Developments in Aprotic and Protic Ionic Liquids: Physical Chemistry and Applications. *Acc. Chem. Res.* **2007**, *40*, 1228−1236.
(34) Yamada, M.; Honma, I. Anhydrous Proton Conducting Polymer Electrolytes Based on Poly(Vinylphosphonic Acid)-Heterocycle Composite Material. *Polymer* **2005**, *46*, 2986−2992.
(35) Narayanan, S. R.; Yen, S.-P.; Liu, L.; Greenbaum, S. G. Anhydrous Proton-Conducting Polymeric Electrolytes for Fuel Cells. *J. Phys. Chem. B* **2006**, *110*, 3942−3948.
(36) Aslan, A.; Bozkurt, A. Development and Characterization of Polymer Electrolyte Membranes Based on Ionical Cross-Linked Poly(1-Vinyl-1,2,4 Triazole) and Poly(Vinylphosphonic Acid). *J. Power Sources* **2009**, *191*, 442−447.
(37) Lin, B.; Cheng, S.; Qiu, L.; Yan, F.; Shang, S.; Lu, J. Protic Ionic Liquid-Based Hybrid Proton-Conducting Membranes for Anhydrous Proton Exchange Membrane Application. *Chem. Mater.* **2010**, *22*, 1807−1813.
(38) Kim, S. Y.; Kim, S.; Park, M. J. Enhanced Proton Transport in Nanostructured Polymer Electrolyte/Ionic Liquid Membranes under Water-Free Conditions. *Nat. Commun.* **2010**, *1*, 88.
(39) Hoarfrost, M. L.; Segalman, R. A. Ionic Conductivity of Nanostructured Block Copolymer/Ionic Liquid Membranes. *Macromolecules* **2011**, *44*, 5281−5288.
(40) Jung, H. Y.; Kim, S. Y.; Kim, O.; Park, M. J. Effect of the Protogenic Group on the Phase Behavior and Ion Transport Properties of Acid-Bearing Block Copolymers. *Macromolecules* **2015**, *48*, 6142−6152.
(41) Chopade, S. A.; So, S.; Hillmyer, M. A.; Lodge, T. P. Anhydrous Proton Conducting Polymer Electrolyte Membranes via Polymerization-Induced Microphase Separation. *ACS Appl. Mater. Interfaces* **2016**, *8*, 6200−6210.
(42) Kajita, T.; Tanaka, H.; Noro, A.; Matsushita, Y.; Nakamura, N. Acidic Liquid-Swollen Polymer Membranes Exhibiting Anhydrous Proton Conductivity Higher than 100 mS cm^{-1} at around 100 °C. *J. Mater. Chem. A* **2019**, *7*, 15585−15592.
(43) Kajita, T.; Noro, A.; Seki, T.; Matsushita, Y.; Nakamura, N. Acidity Effects of Medium Fluids on Anhydrous Proton Conductivity of Acid-Swollen Block Polymer Electrolyte Membranes. *RSC Adv.* **2021**, *11*, 19012−19020.
(44) Darling, H. E. Conductivity of Sulfuric Acid Solutions. *J. Chem. Eng. Data* **1964**, *9*, 421−426.
(45) Matyjaszewski, K.; Xia, J. Atom Transfer Radical Polymerization. *Chem. Rev.* **2001**, *101*, 2921−2990.
(46) Moad, G.; Rizzardo, E.; Thang, S. H. Living Radical Polymerization by the RAFT Process − A Third Update. *Aust. J. Chem.* **2012**, *65*, 985.
(47) Leibler, L. Theory of Microphase Separation in Block Copolymers. *Macromolecules* **1980**, *13*, 1602−1617.
(48) Matsen, M. W.; Bates, F. S. Unifying Weak- and Strong-Segregation Block Copolymer Theories. *Macromolecules* **1996**, *29*, 1091−1098.
(49) Lodge, T. P. A Unique Platform for Materials Design. *Science* **2008**, *321*, 50−51.
(50) Chiefari, J.; Chong, Y. K.; Ercole, F.; Krstina, J.; Jeffery, J.; Le, T. P. T.; Mayadunne, R. T. A.; Meijs, G. F.; Moad, C. L.; Moad, G.; Rizzardo, E.; Thang, S. H. Living Free-Radical Polymerization by Reversible Addition−Fragmentation Chain Transfer: The RAFT Process. *Macromolecules* **1998**, *31*, 5559−5562.
(51) Lai, J. T.; Filla, D.; Shea, R. Functional Polymers from Novel Carboxyl-Terminated Trithiocarbonates as Highly Efficient RAFT Agents. *Macromolecules* **2002**, *35*, 6754−6756.
(52) Noro, A.; Higuchi, K.; Sageshima, Y.; Matsushita, Y. Preparation and Morphology of Hybrids Composed of a Block Copolymer and Semiconductor Nanoparticles via Hydrogen Bonding. *Macromolecules* **2012**, *45*, 8013−8020.
(53) Noro, A.; Tomita, Y.; Shinohara, Y.; Sageshima, Y.; Walish, J. J.; Matsushita, Y.; Thomas, E. L. Photonic Block Copolymer Films Swollen with an Ionic Liquid. *Macromolecules* **2014**, *47*, 4103−4109.
(54) Noro, A.; Tomita, Y.; Matsushita, Y.; Thomas, E. L. Enthalpy-Driven Swelling of Photonic Block Polymer Films. *Macromolecules* **2016**, *49*, 8971−8979.
(55) Hayashi, M.; Noro, A.; Matsushita, Y. Highly Extensible Supramolecular Elastomers with Large Stress Generation Capability Originating from Multiple Hydrogen Bonds on the Long Soft Network Strands. *Macromol. Rapid Commun.* **2016**, *37*, 678−684.
(56) Kajita, T.; Noro, A.; Oda, R.; Hashimoto, S. Highly Impact-Resistant Block Polymer-Based Thermoplastic Elastomers with an Ionically Functionalized Rubber Phase. *ACS Omega* **2022**, *7*, 2821−2830.
(57) Weber, R. L.; Ye, Y.; Banik, S. M.; Elabd, Y. A.; Hickner, M. A.; Mahanthappa, M. K. Thermal and Ion Transport Properties of Hydrophilic and Hydrophobic Polymerized Styrenic Imidazolium Ionic Liquids. *J. Polym. Sci., Part B: Polym. Phys.* **2011**, *49*, 1287−1296.
(58) Noro, A.; Sageshima, Y.; Arai, S.; Matsushita, Y. Preparation and Morphology Control of Block Copolymer/Metal Salt Hybrids via Solvent-Casting by Using a Solvent with Coordination Ability. *Macromolecules* **2010**, *43*, 5358−5364.
(59) Noro, A.; Asai, H.; Higuchi, K.; Matsushita, Y. Self-Assembled Hybrids Composed of Block Copolymer/Porphyrin−Metal Complex via Hydrogen Bonding. *ACS Appl. Polym. Mater.* **2019**, *1*, 3432−3442.
(60) Matsen, M. W. Polydispersity-Induced Macrophase Separation in Diblock Copolymer Melts. *Phys. Rev. Lett.* **2007**, *99*, No. 148304.
(61) Lynd, N. A.; Meuler, A. J.; Hillmyer, M. A. Polydispersity and Block Copolymer Self-Assembly. *Prog. Polym. Sci.* **2008**, *33*, 875−893.
(62) Widin, J. M.; Schmitt, A. K.; Schmitt, A. L.; Im, K.; Mahanthappa, M. K. Unexpected Consequences of Block Polydispersity on the Self-Assembly of ABA Triblock Copolymers. *J. Am. Chem. Soc.* **2012**, *134*, 3834−3844.
(63) Sakurai, S.; Kawada, H.; Hashimoto, T.; Fetters, L. J. Thermoreversible Morphology Transition between Spherical and Cylindrical Microdomains of Block Copolymers. *Macromolecules* **1993**, *26*, 5796−5802.
(64) Sakamoto, N.; Hashimoto, T.; Han, C. D.; Kim, D.; Vaidya, N. Y. Order−Order and Order−Disorder Transitions in a Polystyrene-*block*-Polyisoprene-*block*-Polystyrene Copolymer. *Macromolecules* **1997**, *30*, 1621−1632.
(65) Yashima, E.; Matsushima, T.; Okamoto, Y. Chirality Assignment of Amines and Amino Alcohols Based on Circular Dichroism Induced by Helix Formation of a Stereoregular Poly((4-Carboxyphenyl)Acetylene) through Acid-Base Complexation. *J. Am. Chem. Soc.* **1997**, *119*, 6345−6359.
(66) Nunes, R. W.; Martin, J. R.; Johnson, J. F. Influence of Molecular Weight and Molecular Weight Distribution on Mechanical Properties of Polymers. *Polym. Eng. Sci.* **1982**, *22*, 205−228.

https://doi.org/10.1021/acsomega.2c06514
ACS Omega 2023, 8, 1121−1130